

Learning a Neural 3D Texture Space from 2D Exemplars

Philipp Henzler¹

p.henzler@cs.ucl.ac.uk

Niloy J. Mitra^{1,2}

n.mitra@cs.ucl.ac.uk

Tobias Ritschel¹

t.ritschel@ucl.ac.uk

¹University College London, ²Adobe

Abstract

We propose a generative model of 2D and 3D natural textures with diversity, visual fidelity and at high computational efficiency. This is enabled by a family of methods that extend ideas from classic stochastic procedural texturing (Perlin noise) to learned, deep, non-linearities. The key idea is a hard-coded, tunable and differentiable step that feeds multiple transformed random 2D or 3D fields into an MLP that can be sampled over infinite domains. Our model encodes all exemplars from a diverse set of textures without a need to be re-trained for each exemplar. Applications include texture interpolation, and learning 3D textures from 2D exemplars. Project website: geometry.cs.ucl.ac.uk/projects/2019/neuraltexture

1. Introduction

Textures are stochastic variations of attributes over 2D or 3D space with applications in both image understanding and synthesis. This paper suggests a generative model of natural textures. Previous texture models either capture a single exemplar (e. g., wood) alone or address non-stochastic (stationary) variation of appearance across space: Which location on a chair should have a wood color? Which should be cloth? Which metal?, etc. Our work combines these two complementary views.

Requirements We design the family of methods with several requirements in mind: completeness, generativeness, compactness, interpolation, infinite domains, diversity, infinite zoom, and high speed.

A space of textures is *complete*, if every natural texture has a compact code \mathbf{z} in that embedding. To be *generative*, every texture code should map to a useful texture. This is important for intuitive design where a user manipulates the texture code and expects the outcome to be a texture. *Compactness* is achieved if codes are low-dimensional. We also demand the method to provide *interpolation*: texture generated at coordinates between \mathbf{z}_1 and \mathbf{z}_2 should also be valid.

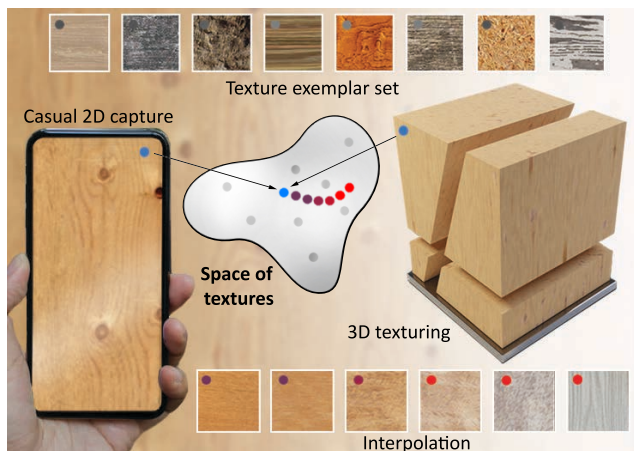


Figure 1. Our approach allows casually captured 2D textures (blue) to be mapped to latent texture codes which can be decoded in 3D for synthesis, design and interpolated (blue-red).

This is important for design or when storing texture codes into a (low-resolution) 2D image, 3D volume or at mesh vertices and then wishing to interpolate it. The first four points are typical for generative modelling; achieving them jointly while meeting more texture-specific requirements (stochasticity, efficiency) is our key contribution.

First, we want to support *infinite domains*: Holding the texture code \mathbf{p} fixed, we want to be able to query this texture so that a patch around any position \mathbf{x} has the statistics of the exemplar. This is important for querying the texture in graphics applications for extended virtual worlds like the grass on a football field which has a vast extend compared to the texture exemplar.

Second, for visual fidelity, the statistics under which textures are *similar* to the exemplar. The Gram matrix of VGG activations is one established metric for this similarity [5].

Third, *infinite zoom* means each texture should have variations on a wide range of scales and not be limited to any fixed resolution that can be held in memory. This is required to zoom into details of geometry and appreciate the fine variation such as wood grains, etc. In practice, we are limited by the frequency content of the exemplars we train on, but the

method should not impose any limitations across scales.

Fourth and finally, our aim is *computational efficiency*: the texture needs to be queryable without requiring prohibitive amounts of memory or time, in any dimension. Ideally, it would be constant in both and parallel. This rules out simple convolutional neural networks, that do not scale favorable in memory consumption to 3D.

2. Previous Work

Capturing the variations of nature using stochastic on many scales has a long history [13]. Making noise useful for graphics and vision is due to Perlin’s 1995 work [16]. Here, textures are generated by computing noise at different frequencies and mixing it with linear weights. A key benefit is that this noise can be evaluated in 2D as well as in 3D making it popular for many graphics applications.

Computer vision typically had looked into generating textures from exemplars, such as by non-parametric sampling [4], vector quantization [23], optimization [11] or nearest-neighbour field synthesis (PatchMatch [2]) with applications in in-painting and also (3D) graphics. Typically, achieving spatial and temporal coherence as well as scalability to fine spatial details remains a challenge. Such classic methods cater to the requirements of human texture perception as stated by Julesz [8]: a texture is an image full of features that in some representation have the same statistics.

The next level of quality was achieved when representations became learned, such as the internal activations of the VGG network [20]. Neural style transfer [5] looked into the statistics of those features, in particular, their Gram matrices. By optimizing over pixel values, these approaches could produce images with the desired texture properties. If these properties are conditioned on existing image structures, the process is referred to as style transfer. VGG was also used for optimization-based multi-scale texture synthesis [18]. A drawback is, that such methods perform an optimization for every exemplar.

Ulyanov et al. [21] and Johnson et al. [7] have proposed networks that directly produce the texture without optimization. While now a network generated the texture, it was still limited to one exemplar, and no diversity was demonstrated. However, noise at different resolutions [16] is input to these methods, also an inspiration to our work. Follow up work [22] has addressed exactly this difficulty by introducing an explicit diversity term i. e., asking all results in a batch to be different. Unfortunately, this frequently introduces mid-frequency oscillations of brightness that appear admissible to VGG instead of producing true diversity. In our work, we achieve diversity, by restricting the networks input to stochastic values only, i. e., diversity-by-construction

A certain confusion can be noted around the term “texture”. In the human vision [8] and computer vision literature [4, 6], it exclusively refers to stochastic variation. In

computer graphics, e. g., OpenGL, “texture” can model both stochastic and non-stochastic variation of color. For example, Visual Object Networks [27] generate a voxel representation of shape and diffuse albedo and refer to the localized color appearance, e. g., wheels of a car are dark, the rim are silver, etc., as “texture”. Similar, Oechsle et al. [15] use an implicit function to model this variation of appearance in details beyond voxel resolution. Our comparison will show, how methods tackling space of non-stochastic texture variation [15, 27], unfortunately are not suitable to model stochastic appearance. Our work is progress towards learning spaces of both stochastic and non-stochastic textures.

Some work has used adversarial training to capture the essence of textures [19, 3], including the non-stationary case [26] or even inside a single image [19]. In particular StyleGAN [9] generates images with details by transforming noise in adversarial training. We avoid the challenges of adversarial training but learn a NN to produce VGG statistics directly.

Aittala et al. [1] have extended Gatsy et al.’s 2015 [5] approach to not only generate color, but also ensembles of 2D BRDF model parameter maps from single 2D exemplars. Our approach is compatible with this approach, for example to generate 3D bump, specular, etc. maps relevant for graphics, but from 2D input.

At any rate, none of the texture works, be it graphics or vision [16, 5, 21, 4, 2, 24, 25] generate a space of textures, such as we suggest here, but all work on a single one while the ones that work on a space of exemplars [27, 15] do not create stochastic textures. Our work closes this gap, by creating a space of stochastic textures. The graphics community however has looked into generating spaces of textures [14], which we here revisit from a deep learning perspective. Their method deforms all pairs of exemplars to each other and constructs a graph with edges that are admissible for interpolation when there is evidence that the warping succeeded. To blend between them, histogram adjustments are made. Consequently, interpolation between exemplars does not take a straight path from another, but traverses just admissible observations. Our approach is complementary, as we could also construct more admissible paths in latent space interpolation.

Finally, all these methods require to learn the texture in the same space it will be used (2D), while our approach can operate in any dimension and across dimensions, including the important case of generating procedural 3D solid textures from 2D observations [10] or slices [17] only.

Summary The state of the art is summarized in Tbl. 1.

Rows list different methods while columns address different aspect of each method. A method is “Diverse” if more than a single exemplar can be produced. MLP is not diverse as the absolute position allows overfitting. We denote

Table 1. Comparison of texture synthesis methods. Please see text for refined definition of the rows and columns.

Method		Diverse	Details	Speed	3D	Quality	Space	2D-to-3D
• Perlin	perlin	✓	✓	✓	✓	×	×	×
• Perlin + transform	perlinT	✓	✓	✓	✓	×	×	×
• CNN	cnn	×	×	×	×	✓	×	×
• CNN + diversity	cnnD	✓	×	×	×	×	×	×
• MLP	mlp	×	×	✓	✓	×	×	✓
• Ours + position	oursP	×	✓	✓	✓	×	✓	✓
• Ours - transform	oursNoT	×	×	✓	✓	✓	✓	✓
• Ours	ours	✓	✓	✓	✓	✓	✓	✓

a method to have “Detail” if it can produce features on all scales. CNN does not have details, as, in particular in 3D, it needs to represent the entire domain in memory, while MLPs and ours are point operations. “Speed” refers to computational efficiency. Due to high bandwidth and lacking data parallelism, a CNN, in particular in 3D, is less efficient than ours and CNNs. This also prevents application to “3D”. “Quality” refers to visual fidelity, a subjective property. CNN, MLP and ours achieve this, but Perlin is too simple a model. CNN with diversity [22] still have decent quality, not worse than ours, but a step back from [21]. Our approach creates a “Space” of a class of textures, while all others only work with a single exemplar. Finally, our approach allows to learn from a single 2D observation i. e., 2D-to-3D. MLP, in texture fields are also learned from 2D images, but these are multiple images of one exemplar, and pixels are labeled with depth.

3. Overview

The key idea of our method is to read several infinite 2D or 3D random fields that differ by learned transformations and feed their values into an MLP to match desired statistics. This process is conditioned on 2D exemplar images. All this is jointly trained on a set of 2D textures images.

This proceeds in two steps: *encoding* and *decoding* (Fig. 2). Encoding g maps an exemplars y from the distribution of natural textures in the *source domain* (2D) to the latent texture code $z = g(y)$. These codes z are fed into a decoder $f(x|z)$ that re-synthesizes single-position samples in the *target domain* (2D or 3D). The decoder is evaluated for a regular grid of points x in random 2D slices of the target domain to produce common “slice” images. These slice images can then be compared to the exemplar y using a texture difference metric defined in the source domain.

Encoding Exemplars are given as 2D images. The encoding is a common convolutional encoder mapping the image with a high number of exemplar pixels to compact latent codes. All results use a latent space of size 8, so $z \in \mathbb{R}^8$.

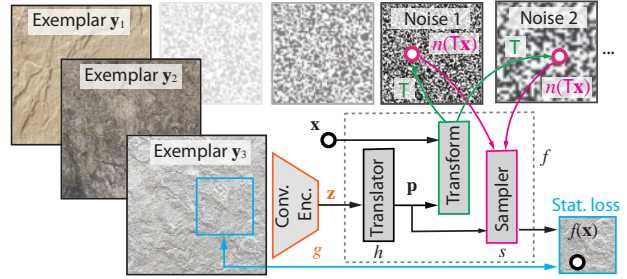


Figure 2. Overview of our approach, comprising of three main parts: The first is an encoder g that takes as input texture images y and generates a compact latent code z (orange). A small translation network h converts this latent code into parameters p that condition a non-convolutional (MLP) decoder (dotted) f that takes noise sampled with learned transformations (green) and maps this to appearance (pink) that has the same statistics as the exemplar (blue).

Please see the supplemental for the definition.

Decoding We found it beneficial to split the decoder $f = s(x|h(z))$ into two parts: a *translator* called h and a *sampler* named s . The translator h maps the latent texture code z into a different, probably larger, redundant but more useful set of parameters p and is executed only once for every texture code, while the sampler is executed many positions x , i. e., pixels. We write conditioned-on- p as the texture code z and hence the translated parameters $p = h(z)$ are fixed when sampling space x .

Metric We use the Gram matrix of VGG feature activations [5, 7, 22, 21, 1] of random 2D slices through the target domain (which might have more spatial or temporal variation). If the source and target domain are the same (synthesizing 2D textures from 2D exemplars) this operation is the identity. However, it also allows for the important condition in which the target domain has more dimensions than the source domain, such as learning 3D from 2D exemplars.

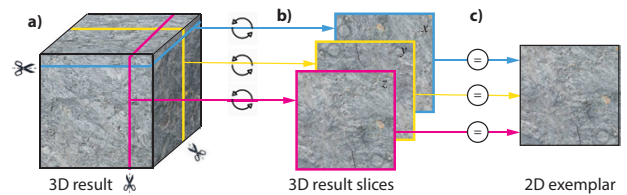


Figure 3. Sliced loss for learning 3D procedural textures from 2D exemplars: Our method, as it is non-convolutional, can sample the 3D texture (a) at arbitrary 3D positions. This enables to also sample arbitrary 2D slices (b). For learning, this allows to simply slice 3D space along the three major axes (red, yellow, blue) and ask each slice to have the same VGG statistics as the exemplar (c).

Training Our method can be used to either fit a *single* exemplar or an entire *space* of textures. In the single mode, no parameters of the encoder g are trained. Instead, we directly optimize for the tuple $\theta = \{\theta_s, \mathbf{p}\}$ i. e., the parameters \mathbf{p} and the tunable parameters θ_s . When learning the entire space of textures, the full cascade of encoder g , translator h and decoder f are trained, i. e., $\theta = \{\theta_g, \theta_h, \theta_s\}$.

Encoder, translator and sampler are trained jointly. In each training step, random patches of 128×128 pixels are cut out of the exemplar with wrap-around and used as the target.

4. Learning stochastic space coloring

Here we will introduce different implementations of samplers s which “color” 2D or 3D space at position \mathbf{x} . We will discuss pros and cons in respect to the requirements from the introduction, ultimately leading to our approach.

Perlin noise is a simple and effective method to generate natural textures in 2D or 3D [16], defined as

$$s(\mathbf{x}|\mathbf{p}) = \sum_{i=1}^{n_o} \text{noise}_i(2^{-i}\mathbf{x}) \otimes w_i, \quad (1)$$

$$\mathbf{p} = \{w_0, w_1, \dots\}$$

where w are the RGB weights for n_o different noise functions noise_i which return bilinearly-sampled RGB values from an integer grid. \otimes is channel-wise multiplication. Throughout this paper, noise is unit Gaussian.

Here, \mathbf{p} is a list of all linear per-layer RGB weights e. g., an 8×3 vector for the $n_o = 8$ octaves we use. This is a simple latent code, but we will see increasingly complex ones later. Also our encoder g is designed such that it can cater to all decoders, even classic Perlin noise i. e., we can also create a space of textures with a Perlin noise back-end.

Coordinate \mathbf{x} are divided by factors of two (octaves), so with increasing i , increasingly smooth noises are combined. This is motivated well in the spectra of natural signals [13, 16], but also limiting. Further, the linear scaling allows re-scaling the noise to have different colors, yet no linear operation can reshape each distribution and they are combined linearly again. Our work seeks to overcome these two limitations, but trying to retain the desirable properties of Perlin noise: simplicity and computational efficiency as well as generalization to 3D.

Transformed Perlin relaxes the scaling by powers of two

$$s(\mathbf{x}|\mathbf{p}) = \sum_{i=1}^{n_o} \text{noise}_i(\mathbb{T}_i\mathbf{x}) \otimes w_i, \quad (2)$$

$$\mathbf{p} = \{w_0, w_1, \dots, \mathbb{T}_0, \mathbb{T}_1, \dots\}$$

by allowing each noise i to be independently scaled by its own transformation matrix \mathbb{T}_i . Please note, that the choice of noise frequency is now achieved by scaling the coordinates reading the noise. This allows to make use of anisotropic scaling for elongated structures, different orientations or multiple random inputs at the same scale.

CNN directly learns convolutions to turn a random seed into a texture [22]

$$s(\mathbf{x}|\mathbf{p}) = \text{cnn}(\mathbf{x}|\mathbf{u}) \quad (3)$$

$$\mathbf{p} = \{\mathbf{u}\}.$$

Input to the CNN is a random vector that is the filtered and up-sampled in several cascades. The CNN is conditioned on \mathbf{u} without additional translation. Their visual quality is stunning, CNNs are powerful and the loss is now very well able to capture perceptually important texture features, i. e., CNNs are a target to chase for us in 2D in terms of quality. However, there are two main limitations of this approach we seek to lift: efficiency and diversity.

CNNs do not scale well to 3D in high resolutions. To compute intermediate features at \mathbf{x} , they need to have access to neighbours. While this is effective and output-sensitive in 2D, it is not in 3D: we need results for 2D surfaces embedded in 3D, and do so in spatial high resolution (say 1024×1024), but this requires CNNs to compute a full 3D volume with the same order of pixels. While in 2D partial outputs can be achieved with sliding windows, it is less clear how to slide a window in 3D, such that it covers all points required to cover all 3D points that are part of the visible surface.

The second issue is diversity: CNNs are great for producing a re-synthesis of the input exemplar, but it has not been demonstrated that changing the input noise will lead to variation in the output in most classic works [21, 7] and in classic style transfer [5] diversity is eventually introduced due to the randomness in SGD, if at all. 2017 work by Ulyanov and colleagues [22] explicitly incentivizes diversity in the loss. The main idea is to increase the pixel variance inside all exemplars produced in one batch. Regrettably, this often is achieved by merely shifting the same one exemplar slightly spatially or introducing random brightness fluctuations. We will include this approach in our comparison.

MLP maps a 3D coordinate to appearance, as in

$$s(\mathbf{x}|\mathbf{p}) = \text{mlp}(\mathbf{x}|\mathbf{u}) \quad (4)$$

$$\mathbf{p} = \{\mathbf{u}\}.$$

Again, the MLP is conditioned on \mathbf{u} . Texture-fields [15] have used this approach to produce what they call “texture”, detailed and high-quality appearance decoration of 3D surfaces, but what was probably not even intended is to produce diversity or any stochastic result at all. At least, there is

no parameter that introduces any randomness, so all results are identical. We took inspiration in their work, as it makes use of 3D point operation, that do not require accessing any neighbours and no intermediate storage for features in any dimensions, including 3D. It hence reduces bandwidth compared to CNN, is perfectly data-parallel and scalable. The only thing missing to make it our colorization operator required to create a space and go from 2D exemplars to 3D textures is stochasticity. We will add this next.

Ours combines the noise from transformed Perlin for stochasticity, the losses used in style and texture synthesis CNNs for quality as well as the point operations in MLPs for efficiency as follows:

$$s(\mathbf{x}|\mathbf{p}) = \text{mlp}(\text{noise}_1(\mathbf{T}_1\mathbf{x}), \text{noise}_2(\mathbf{T}_2\mathbf{x}), \dots | \mathbf{u})$$

$$\mathbf{p} = \{\mathbf{u}, \mathbf{T}_1, \mathbf{T}_2, \dots\}. \quad (5)$$

Different from MLPs that take the coordinate \mathbf{x} as input, position itself is hidden. Instead of position, we take multiple copies of spatially smooth noise $\text{noise}(\mathbf{x})$ as input, with explicit control of how the noise is aligned in space expressed by the matrix \mathbf{T} . Hence, the MLP requires to map the entire distribution of noise values such that it suits the loss, resulting in build-in diversity: a new random field will produce a new instance of the texture.

In particular, the MLP takes in two kinds of values: such values that control the transformations \mathbf{T}_1, \dots ($8 \times 4 = 32$ for $n_o = 8$ octaves) and others (32) that condition the MLP itself. The MLP has four layers, each one with 128 units. Each layer has a ReLU and the last layer is 3-valued RGB.

Non-stochastic ablation seeks to investigate what happens if we do not limit our approach to access random variables $\text{noise}(\mathbf{x})$, but also provide access to deterministic information \mathbf{x} :

$$s(\mathbf{x}|\mathbf{p}) = \text{mlp}(\text{noise}_1(2^{-0}\mathbf{x}), \text{noise}_2(2^{-1}\mathbf{x}), \dots | \mathbf{x} | \mathbf{u})$$

$$\mathbf{p} = \{\mathbf{u}\}, \quad (6)$$

is the same as MLP, but with access to noise. We will see that this effectively removes diversity.

Non-transformed ablation evaluates, if our method were to read only from multi-scale noise without control over how it is transformed. Its definition

$$s(\mathbf{x}|\mathbf{p}) = \text{mlp}(\text{noise}_1(2^{-0}\mathbf{x}), \text{noise}_2(2^{-1}\mathbf{x}), \dots | \mathbf{u})$$

$$\mathbf{p} = \{\mathbf{u}\}, \quad (7)$$

is the same as ours, just that the noise is read at non-transformed coordinates as in classic Perlin noise.

5. Evaluation

Our evaluation covers qualitative (Sec. 5.2) and quantitative (Sec. 5.3) aspects as well as a user study (Sec. 6).

5.1. Protocol

We suggest a data set that for which we explore the relation of different methods, according to different metrics to quantify texture similarity and diversity.

Data set Our data set contains four classes (WOOD, MARBLE, GRASS and RUST) of 2D textures, acquired from internet image sources. All were resampled to the same size of 1024×1024 pixels. Each class contains 100 images.

Methods We compare eight different methods that are competitors, ablations and ours.

As five *competitors* we study variants of Perlin noise, CNNs and MLPs. `perlin` implements Perlin noise (Eq. 1, [16]) and `perlinT` our variant extending it by a linear transformation of coordinates before reading the noise tables (Eq. 2). Next, `cnn` is a classic TextureNet [21] and `cnnD` the extension to incentivise diversity ([22], Eq. 3). `mlp` uses an MLP following Eq. 4.

We study three *ablations*. First, we compare to `oursP` that is our method, but with the absolute position as input and no transform. Second, `oursNoT` omits learning an explicit transform but uses Perlin’s octaves instead (Eq. 7). The final method is `our` method (Eq. 5).

Metrics We evaluate methods in respect to three metrics: similarity and diversity and a joint measure, success.

Similarity is high, if the result produced has the same statistics as the exemplar in terms of L2 differences of VGG Gram matrices. This is identical to the loss used. Similarity is measured on a single exemplar. Similarity is maximized by re-generating the exemplar, but at the expense of diversity.

Diversity is not part of the loss, but can be measured on a set of exemplars produced by a method. We measure diversity by looking at the VGG differences between all pairs of results in a set produced for different random seed. Note, that this does not take into account any reference. Diversity is easily maximized by just producing random VGG responses, yet without similarity.

Success of the entire method is measured as the product of diversity and the maximum style error minus the style error. We apply this metric, as it combines similarity and diversity that are conflicting goals we jointly want to maximize.

Memory and speed are measured at a resolution of 128 pixels/voxels on an Nvidia Titan Xp.

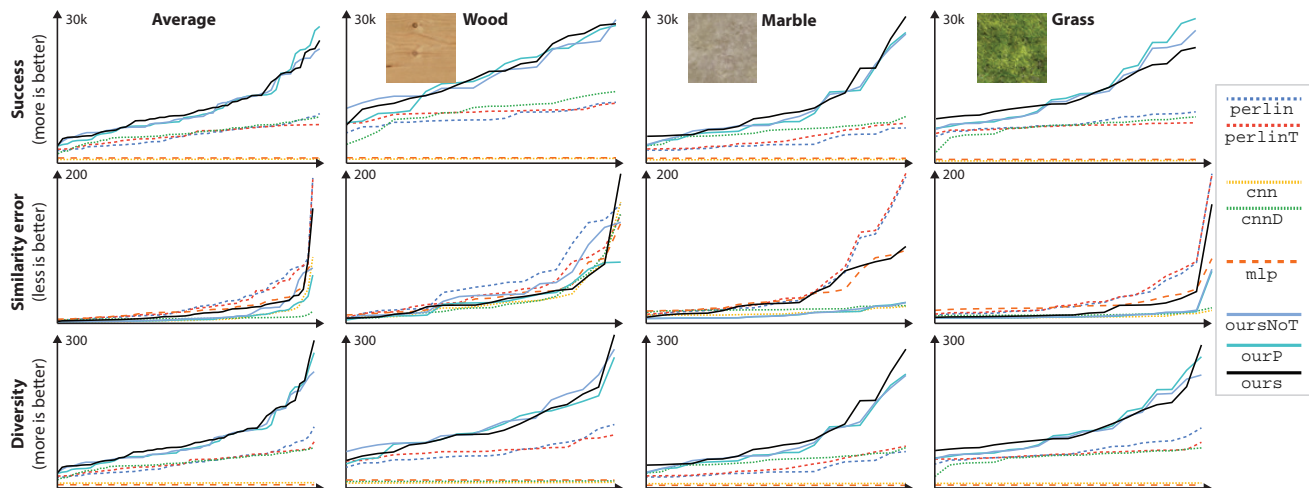
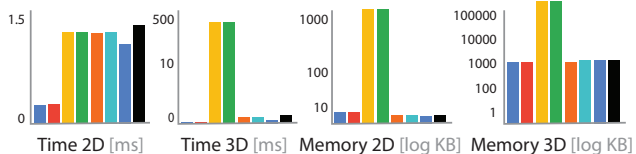


Figure 4. Quantitative evaluation. Each plot shows the histogram of a quantity (from top to bottom: success, style error and diversity) for different data sets (from left to right: all space together, WOOD, MARBLE, GRASS). For a discussion, see the last paragraph in Sec. 5.2.

Table 2. Efficiency in terms of compute time and memory usage in 2D and 3D (columns) for different methods (rows).

Method	Time		Memory	
	2D	3D	2D	3D
perlin	0.18 ms	0.18 ms	65 k	16 M
perlinT	0.25 ms	0.25 ms	65 k	16 M
cnn	1.45 ms	551.59 ms	8,000 k	646 M
cnnD	1.45 ms	551.59 ms	8,000 k	646 M
mlp	1.43 ms	1.43 ms	65 k	16 M
oursP	1.44 ms	1.44 ms	65 k	16 M
oursNoT	1.24 ms	1.24 ms	65 k	16 M
ours	1.55 ms	1.50 ms	65 k	16 M



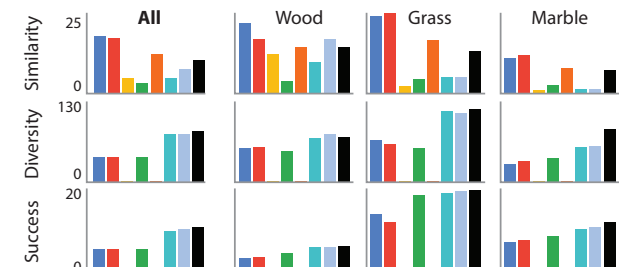
5.2. Quantitative results

Efficiency We first look at computational efficiency in Tbl. 2. We see that our method shares the speed and memory efficiency with Perlin noise and MLPs / Texture Fields [15]. Using a CNN [21, 22] to generate 3D textures as volumes is not practical in terms of memory, even at a modest resolution. Ours scales linear with pixel resolution as an MLP is a point-estimate in any dimension that does not require any memory other than its output. A CNN has to store the internal activations of all layers in memory for information exchange between neighbours.

Fidelity Fig. 4 and Tbl. 3 summarize similarity, diversity and success of all methods in numbers. `ours` method (black) comes best in diversity and success on average across all sets (first column in Tbl. 3 and top first plot in Fig. 4). `cnn`

Table 3. Similarity and diversity for methods on different textures.

Method	ALL			WOOD			GRASS			MARBLE		
	Sim	Div	Suc	Sim	Div	Suc	Sim	Div	Suc	Sim	Div	Suc
perlin	20.6	48.0	7.0	23.8	37.9	4.9	24.6	72.8	18.1	13.3	31.8	7.84
perlinT	19.6	48.2	7.2	18.4	39.6	5.02	25.9	65.6	13.8	14.2	38.4	8.03
cnn	5.4	0.5	7.5	13.4	0.5	0.07	1.9	0.5	0.14	1.1	0.3	0.08
cnnD	3.9	48.2	7.75	3.9	35.2	5.19	4.8	59.2	20.9	3.6	48.8	8.5
mlp	14.1	0.0	7.98	15.7	0.0	0.0	16.7	0.0	0.0	9.6	0.0	0.0
oursP	5.4	93.4	8.23	9.7	67.4	5.33	4.8	126	21.5	1.8	84.5	9.0
oursNoT	8.4	94.5	8.54	18.3	74.7	5.40	5.1	120	21.7	1.9	87.0	9.3
ours	12.1	99.7	8.82	13.3	72.5	5.48	13.6	127	22.1	9.4	98.2	9.6



(yellow) and `cnnD` (green) have better similarity than any of our methods. However, no other method combines similarity with diversity as well as ours. This is visible from the overall leading performance in the final measure, success. This is a substantial achievement, as maximizing for only one goal is trivial: a hypothetical `identity` method produces zero similarity error while a hypothetical `random` method would have infinite diversity.

When looking at the similarity, we see that both a `cnn` and its diverse variant `cnnD` can perform similar variants of Perlin noise produce the largest error. In particular, `perlinT` has a large error, indicating it is not sufficient to merely add a transform. Similar, and `mlp` alone cannot

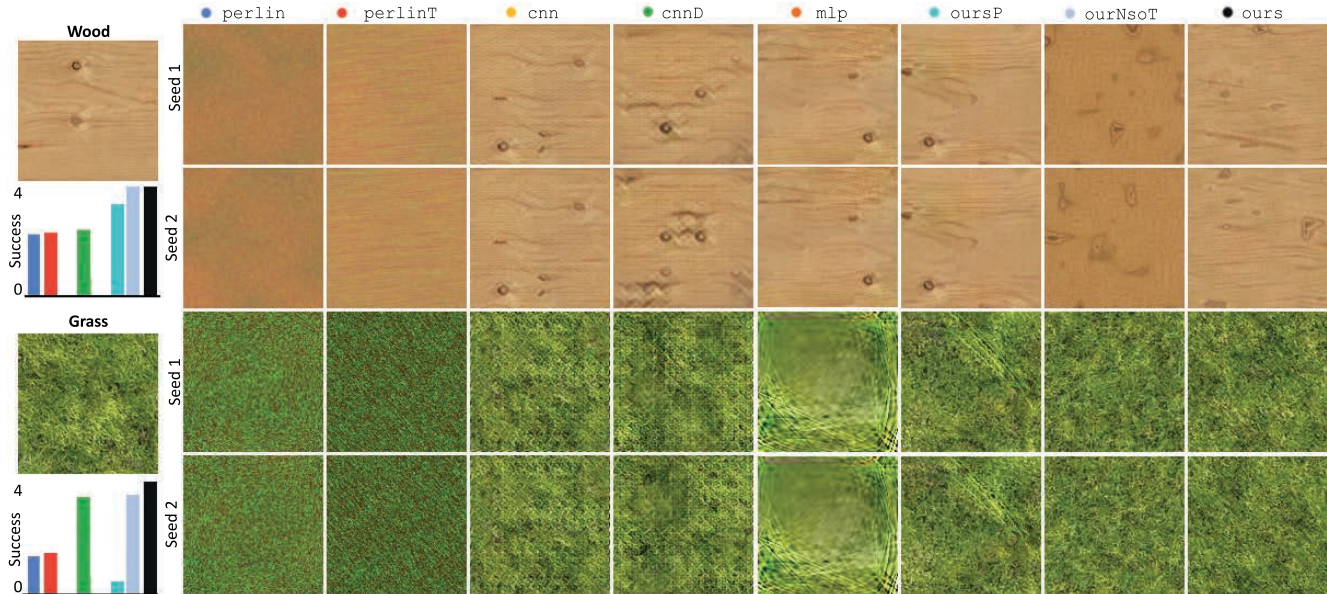


Figure 5. Different methods and the exemplar (columns), as defined in Sec. 5.2, applied to different exemplars (rows). Each row shows, arranged vertically, two re-syntheses with different seeds. Please see the text for discussion.

solve the task, as it has no access to stochastic information and need to fit exactly, which is doable for single exemplars, but impossible for entire spaces. `oursNoT` has error similar to `ours`, but less diversity.

When looking at diversity, it is clear that both `cnn` and `mlp` have no diversity as they either do not have the right loss to incentivize it or have no input to generate it. `perlin` and `perlinT` both create some level of diversity, which is not surprising as they are simple remappings of random numbers. However, they do not manage to span the full VGG space, which only `our` and its ablations can do.

5.3. Qualitative results

Visual examples from the quantitative evaluation on a single exemplar for different methods can be seen in Fig. 5. We see that some methods have diversity when the seed is changed (rows one vs. two and three vs. four) and some do not. Diversity is clear for Perlin and its variant, CNNs with a diversity term and our approach. No diversity is found for MLPs and CNNs. We also note, that CNNs with diversity produce typically shifted copies of the same exemplar, so their diversity is over-estimated by the metric.

A meaningful latent texture code space should also allow for interpolation as seen in Fig. 6, where we took pairs of texture codes in WOOD at the end of each row and interpolated rows in-between. We see, that different paths produce plausible blends, with details appearing and disappearing, which a linear blend (last row) would not have.

Fig. 7 shows a stripe that has been re-synthesized from a single exemplar. We note that the pattern captures the statistics, but does not repeat.



Figure 6. Interpolation of one exemplar (left) into another one (right) in latent space (first three rows) and linear (last row).

Our method does not work on an explicit pixel grid, which allows to zoom into arbitrary fine details as show in Fig. 10, comparing favorable to cubic upsampling. This is particularly useful in 3D, where storing a complete volume to span multiple levels of detail requires prohibitive amounts of memory while ours is output-sensitive.

Fig. 9 documents the ability to reproduce the entire space. We took our MARBLE space and mapped exemplars unobserved at training time to texture codes, from which we reconstruct them, in 2D. We find that our approach reproduces the exemplars faithfully, albeit totally different on the pixel level. Also it spans different kinds of marble.

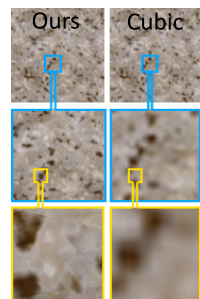


Figure 10. Zooming.

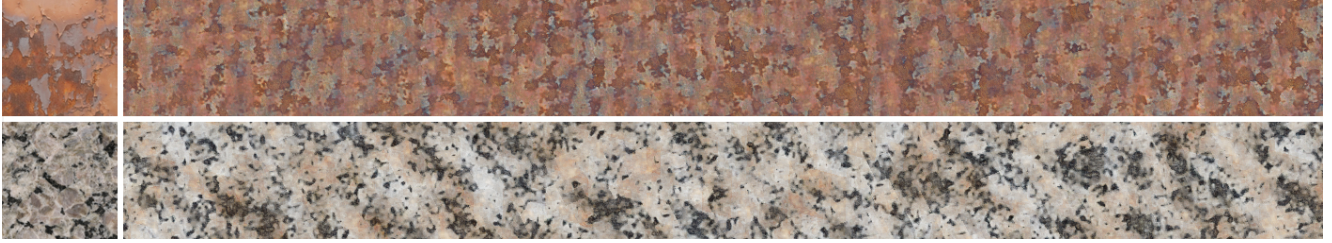


Figure 7. Stripe of re-synthesized two textures (**rows**) from small exemplars on the right. See the supplemental for an animation.

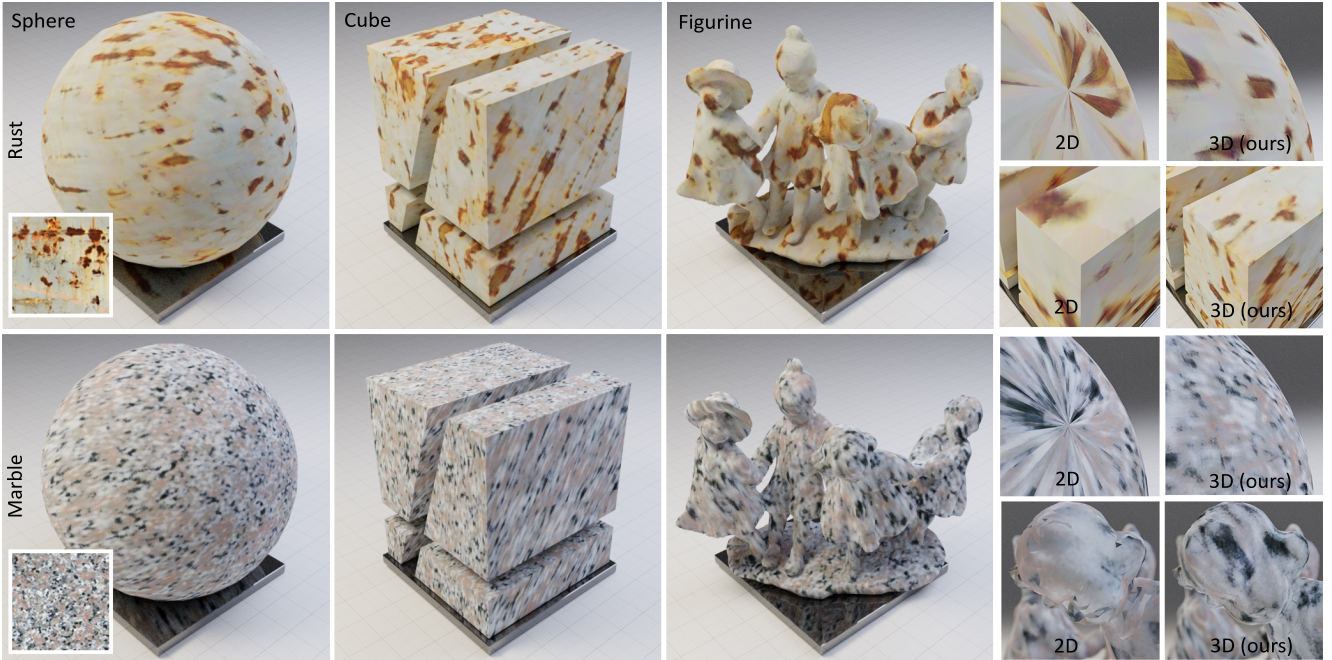


Figure 8. 3D texturing of 3D shapes (**columns**) by 2D exemplars (**rows**). Insets compare ours to 2D texturing. See supplemental for 3D spin.

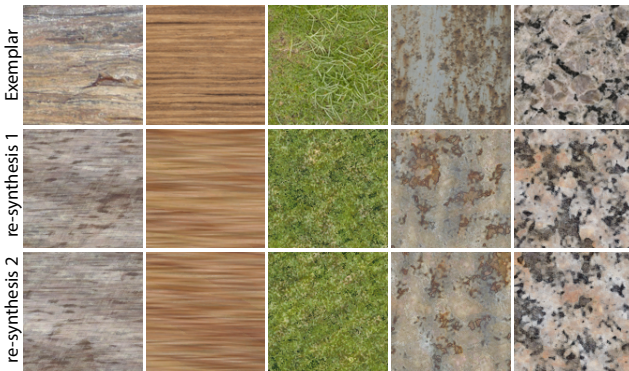


Figure 9. Our reconstruction of WOOD, GRASS, RUST, and MARBLE textures. The first row shows different input exemplars. The second and third row show our reconstruction results with different seeds. This is a projection operation to the space of textures.

Finally, the most distinguished feature of our system is the ability to construct textures and spaces of textures in 3D from 2D exemplars alone. This is shown in Fig. 8. We

first notice, that the textures have been transferred to 3D faithfully, inheriting all the benefits of procedural textures in image synthesis. We can now take any shape, without a texture parametrization and by simply running the NN at each pixel’s 3D coordinate produce a color. We compare to a 2D approach by loading the objects in Blender and applying its state-of-the-art UV mapping approach [12]. Inevitably, a sphere will have discontinuities and poles that can not be resolved in 2D, that are no issue to our 3D approach while both take the same 2D as input.

6. User study

Presenting $M = 144$ pairs of images produced by either `perlinT`, `cnnD`, `mlp`, `oursP`, `oursNoT` and `ours` for one exemplar texture to $N = 28$ subjects and asking which result “they prefer” in a two-alternative forced choice, we find that 16.7% prefer the ground truth, 4.9% `perlinT`, 7.7% `perlinT`, 14.3% `cnn`, 8.8% `cnnD`, 9.4% `mlp`, 10.8% `ourNoT`, 12.9% `ourP` and 10.8% `oursNo` (statistical significance; $p < .1$, binomial test). Given ground truth and

cnns are not diverse, out of all methods that synthesize infinite textures our results are preferred over all other.

7. Conclusion

We have proposed a generative model of natural 3D textures. It is trained on 2D exemplars only, and provides interpolation, synthesis and reconstruction in 3D. The key inspiration is Perlin Noise – now more than 30 years old – revisited with NNs to match complex color relations in 3D according to the statistics of VGG activations in 2D. The approach has the best combination of similarity and diversity compared to a range of published alternatives, that are less computationally efficient.

Reshaping noise to match VGG activations using MLPs can be a scalable solution to other problems in even higher dimensions, such as time, that are difficult for CNNs.

References

- [1] Miika Aittala, Timo Aila, and Jaakko Lehtinen. Reflectance modeling by neural texture synthesis. *ACM Trans. Graph. (Proc. SIGGRAPH)*, 35(4):65, 2016. [2](#), [3](#)
- [2] Connelly Barnes, Eli Shechtman, Adam Finkelstein, and Dan B Goldman. Patchmatch: A randomized correspondence algorithm for structural image editing. *ACM Trans. Graph. (Proc. SIGGRAPH)*, 28(3):24, 2009. [2](#)
- [3] Urs Bergmann, Nikolay Jetchev, and Roland Vollgraf. Learning texture manifolds with the periodic spatial gan. In *J MLR*, pages 469–477, 2017. [2](#)
- [4] Alexei A Efros and Thomas K Leung. Texture synthesis by non-parametric sampling. In *ICCV*, volume 2, 1999. [2](#)
- [5] Leon Gatys, Alexander S Ecker, and Matthias Bethge. Texture synthesis using convolutional neural networks. In *NIPS*, 2015. [1](#), [2](#), [3](#), [4](#)
- [6] Aaron Hertzmann, Charles E Jacobs, Nuria Oliver, Brian Curless, and David H Salesin. Image analogies. In *Proc. SIGGRAPH*, 2001. [2](#)
- [7] Justin Johnson, Alexandre Alahi, and Li Fei-Fei. Perceptual losses for real-time style transfer and super-resolution. In *ECCV*, 2016. [2](#), [3](#), [4](#)
- [8] Bela Julesz. Texture and visual perception. *Scientific American*, 212(2), 1965. [2](#)
- [9] Tero Karras, Samuli Laine, and Timo Aila. A style-based generator architecture for generative adversarial networks. In *CVPR*, pages 4401–4410, 2019. [2](#)
- [10] Johannes Kopf, Chi-Wing Fu, Daniel Cohen-Or, Oliver Deussen, Dani Lischinski, and Tien-Tsin Wong. Solid texture synthesis from 2d exemplars. *ACM Trans. Graph. (Proc. SIGGRAPH)*, 26(3):2, 2007. [2](#)
- [11] Vivek Kwatra, Irfan Essa, Aaron Bobick, and Nipun Kwatra. Texture optimization for example-based synthesis. In *ACM Trans. Graph.*, volume 24, 2005. [2](#)
- [12] Bruno Lévy, Sylvain Petitjean, Nicolas Ray, and Jérôme Maillot. Least squares conformal maps for automatic texture atlas generation. In *ACM Trans Graph.*, volume 21, pages 362–71, 2002. [8](#)
- [13] Benoit B Mandelbrot. *The fractal geometry of nature*, volume 173. WH freeman New York, 1983. [2](#), [4](#)
- [14] Wojciech Matusik, Matthias Zwicker, and Frédo Durand. Texture design using a simplicial complex of morphable textures. *ACM Trans. Graph. (proc. SIGGRAPH)*, 24(3), 2005. [2](#)
- [15] Michael Oechsle, Lars Mescheder, Michael Niemeyer, Thilo Strauss, and Andreas Geiger. Texture fields: Learning texture representations in function space. In *ICCV*, 2019. [2](#), [4](#), [6](#), [11](#)
- [16] Ken Perlin. An image synthesizer. *SIGGRAPH Comput. Graph.*, 19(3), 1985. [2](#), [4](#), [5](#)
- [17] Nico Pietroni, Miguel A Otaduy, Bernd Bickel, Fabio Ganovelli, and Markus Gross. Texturing internal surfaces from a few cross sections. In *Comp. Graph. Forum*, volume 26, 2007. [2](#)
- [18] Omry Sendik and Daniel Cohen-Or. Deep correlations for texture synthesis. *ACM Trans. Graph.*, 36(5):161, 2017. [2](#)
- [19] Tamar Rott Shaham, Tali Dekel, and Tomer Michaeli. Singan: Learning a generative model from a single natural image. In *ICCV*, 2019. [2](#)
- [20] Karen Simonyan and Andrew Zisserman. Very deep convolutional networks for large-scale image recognition. *arXiv preprint arXiv:1409.1556*, 2014. [2](#)
- [21] Dmitry Ulyanov, Vadim Lebedev, Andrea Vedaldi, and Victor S Lempitsky. Texture networks: Feed-forward synthesis of textures and stylized images. In *ICML*, volume 1, page 4, 2016. [2](#), [3](#), [4](#), [5](#), [6](#)
- [22] Dmitry Ulyanov, Andrea Vedaldi, and Victor Lempitsky. Improved texture networks: Maximizing quality and diversity in feed-forward stylization and texture synthesis. In *CVPR*, 2017. [2](#), [3](#), [4](#), [5](#), [6](#), [11](#)
- [23] Li-Yi Wei and Marc Levoy. Fast texture synthesis using tree-structured vector quantization. In *Proc. SIGGRAPH*, 2000. [2](#)
- [24] Wenqi Xian, Patsorn Sangkloy, Varun Agrawal, Amit Raj, Jingwan Lu, Chen Fang, Fisher Yu, and James Hays. Texturegan: Controlling deep image synthesis with texture patches. In *CVPR*, 2018. [2](#)
- [25] Ning Yu, Connelly Barnes, Eli Shechtman, Sohrab Amirghodsi, and Michal Lukac. Texture mixer: A network for controllable synthesis and interpolation of texture. In *CVPR*, 2019. [2](#)

- [26] Yang Zhou, Zhen Zhu, Xiang Bai, Dani Lischinski, Daniel Cohen-Or, and Hui Huang. Non-stationary texture synthesis by adversarial expansion. *arXiv preprint arXiv:1805.04487*, 2018. [2](#)
- [27] Jun-Yan Zhu, Zhoutong Zhang, Chengkai Zhang, Jiajun Wu, Antonio Torralba, Josh Tenenbaum, and Bill Freeman. Visual object networks: image generation with disentangled 3d representations. In *NIPS*, 2018. [2](#)

A. Network Architecture

A.1. Encoder

The architecture for the encoder network remains consistent for both ours and competitor methods. Depending on training for *space*, *single*, *w/o transform* the parameter N changes accordingly.

Table 4. Network architecture for encoder.

Layer	Kernel	Activation	Shape	# params
Input	—	—	3 x 128 x 128	—
Conv	3x3	IN+LReLU	32 x 128 x 128	~1k
Conv	4x4	IN+LReLU	64 x 64 x 64	~32k
Conv	4x4	IN+LReLU	128 x 32 x 32	~130k
Conv	4x4	IN+LReLU	256 x 16 x 16	~524k
Conv	4x4	IN+LReLU	256 x 8 x 8	~1M
Conv	4x4	IN+LReLU	256 x 4 x 4	~1M
Linear	—	—	8	~32k
Linear	—	—	N	~0.5k
# params	—	—		~2.8M

A.2. Sampler

The sampler architecture used for both our and the *mlp* [15] method consists of following convolutional architecture with 1x1 kernels emulating Linear layers:

Table 5. Network architecture for sampler.

Layer	Kernel	Activation	Shape	# params
Input	—	—	N x 128 x 128	—
Conv	1x1	ReLU	128 x 128 x 128	~10k
Conv	1x1	ReLU	128 x 128 x 128	~16.5k
Conv	1x1	ReLU	128 x 128 x 128	~16.5k
Conv	1x1	ReLU	128 x 128 x 128	~16.5k
Conv	1x1	ReLU	128 x 128 x 128	~16.5k
Conv	1x1	ReLU	3 x 128 x 128	~400
# params	—	—		~77k

A.3. CNN

For *cnn* and *cnnD* competitors we use a similar architecture to the proposed method of [22]:

Table 6. Network architecture for convolutional methods.

Layer	Kernel	Activation	Shape	# params
Input	—	—	(32) + 256	—
Linear	—	—	(32) + 256	~80k
Linear	—	—	256	~70k
Reshape	—	—	16 x 4 x 4	—
ConvT	4x4	ReLU	128 x 8 x 8	~32k
ConvT	4x4	ReLU	128 x 16 x 16	~260k
ConvT	4x4	ReLU	128 x 32 x 32	~260k
Upsample	—	—	128 x 64 x 64	—
Conv	3x3	ReLU	64 x 64 x 64	~70k
Upsample	—	—	64 x 128 x 128	—
Conv	3x3	ReLU	3 x 128 x 128	~2k
# params	—	—		~790k

B. Results

Additional results are displayed below.



Figure 11. Results derived from the encoded WOOD space.

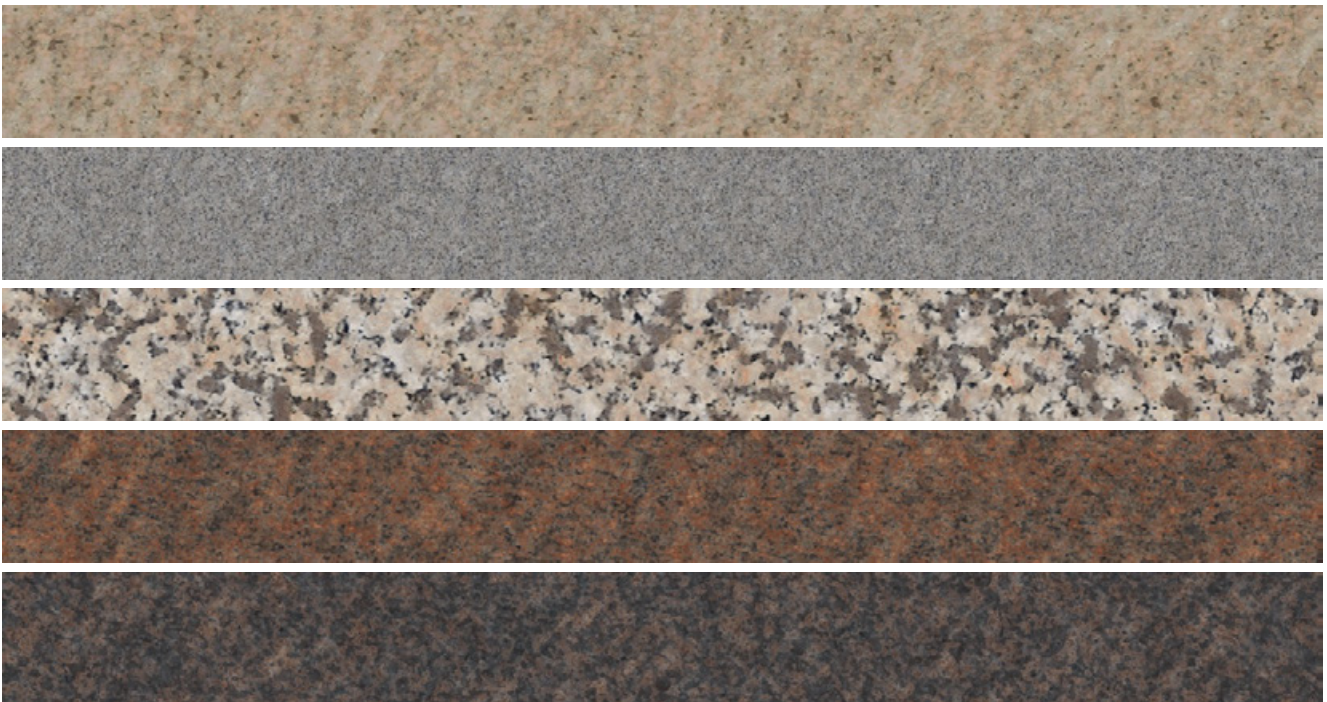


Figure 12. Results derived from the encoded MARBLE space.



Figure 13. Results derived from the encoded GRASS space.

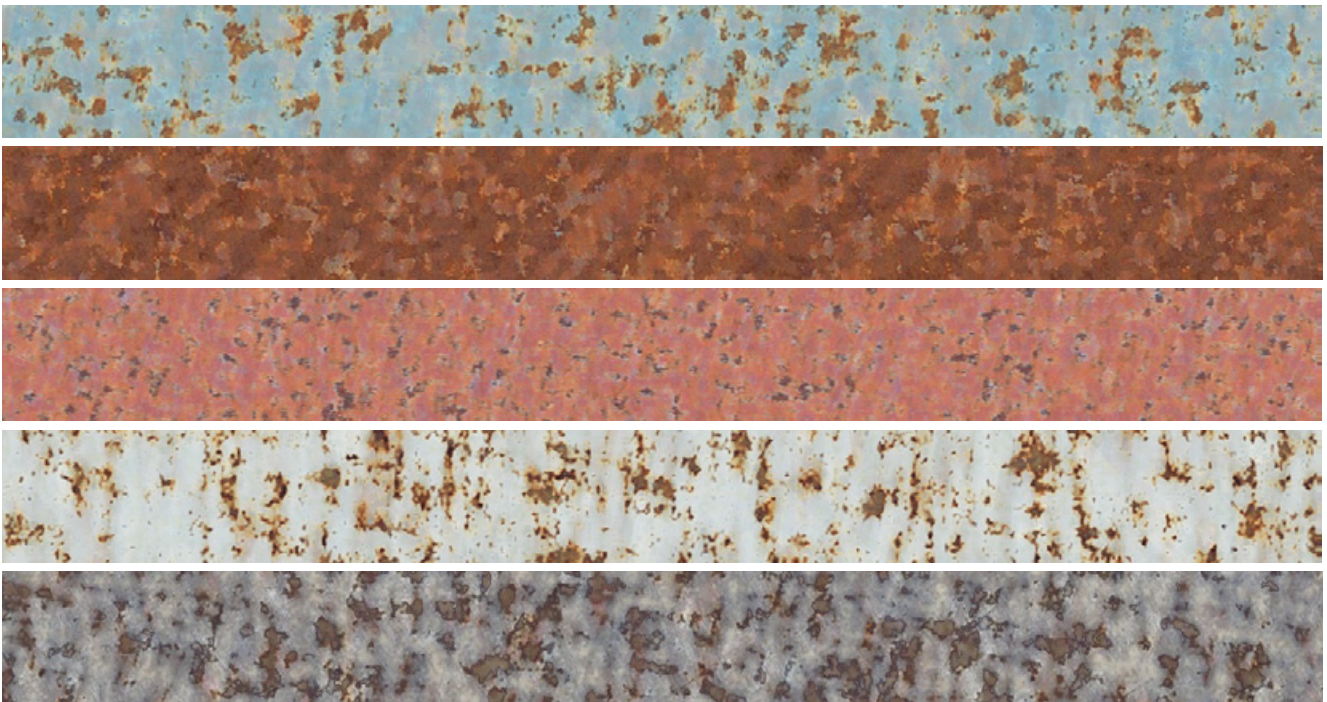


Figure 14. Results derived from the encoded RUST space.



Figure 15. Latent space interpolation from one ground truth wood exemplar (left) into secondary ground truth exemplar (right). Each row corresponds to independent interpolations.

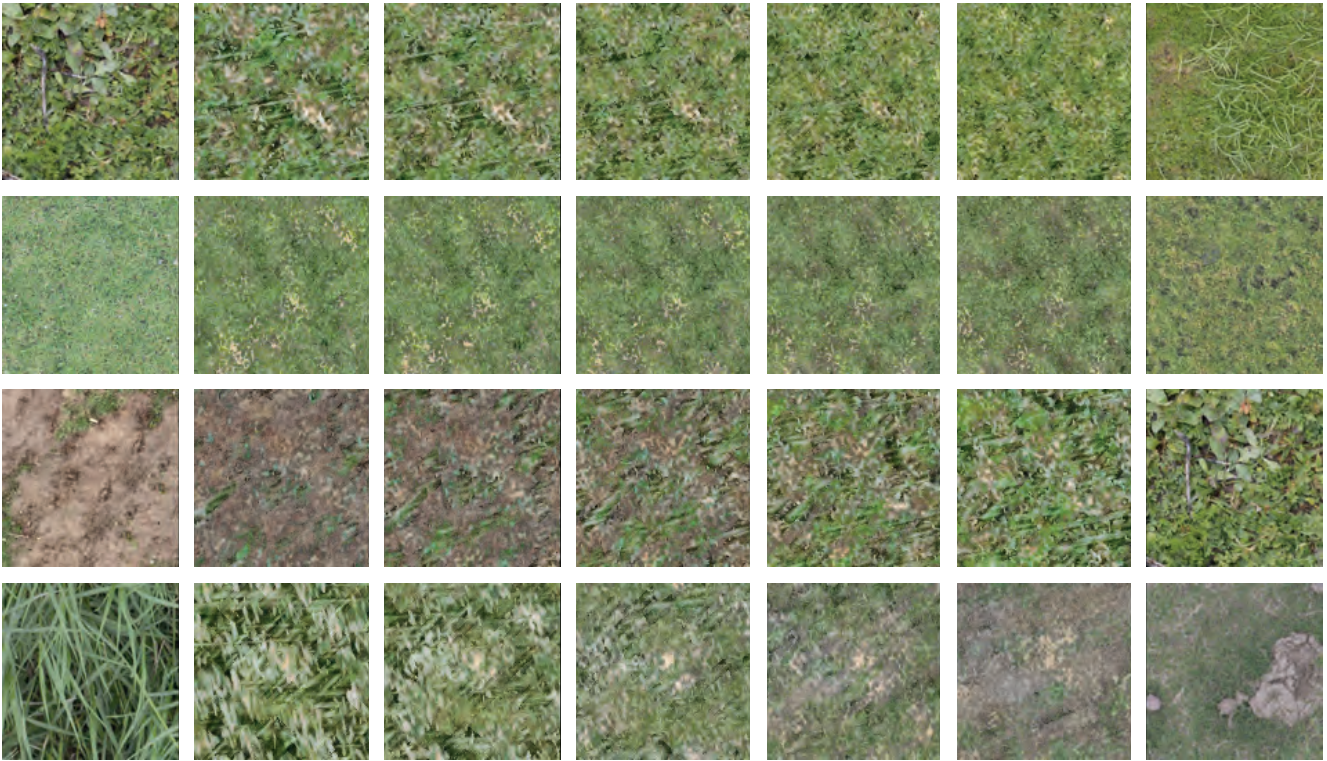


Figure 16. Latent space interpolation from one ground truth grass exemplar (left) into secondary ground truth exemplar (right). Each row corresponds to independent interpolations.



Figure 17. Latent space interpolation from one ground truth marble exemplar (left) into secondary ground truth exemplar (right). Each row corresponds to independent interpolations.

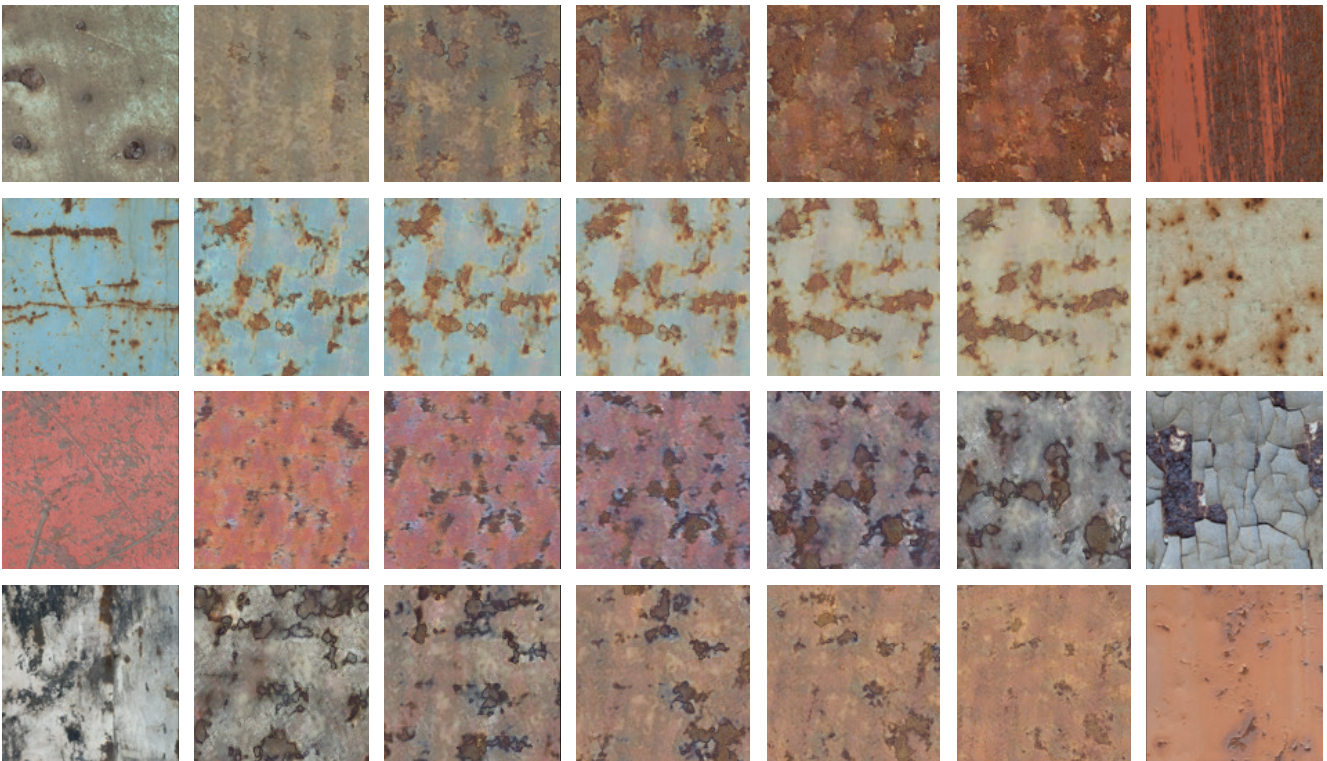


Figure 18. Latent space interpolation from one ground truth rust exemplar (left) into secondary ground truth exemplar (right). Each row corresponds to independent interpolations.